Cephalopod-Inspired Design of Photomechanically Modulated Display Systems for On-Demand Fluorescent Patterning

Huihui Shi, Shuangshuang Wu, Muqing Si, Shuxin Wei, Guoqing Lin, Hao Liu, Weiping Xie, Wei Lu, and Tao Chen**

Cephalopods can display variable body color/patterns upon environmental stimulation via bioelectricity-controlled muscle contraction/expansion of skin chromatophores. However, it remains challenging to produce artificial display analogs that exhibit reversible and rapid switching between multiple expected luminescent patterns, although such systems are very appealing for many practical uses (e.g., data encryption). Inspired by the bioelectromechanical display tactic of cephalopods, in this work, a conceptually new photomechanically modulated fluorescent system that enables on-demand display of fluorescent patterns via a cascading stimulation–mechanical movement–optical output conduction mechanism is presented. Specifically, this biomimetic system comprises a customizable hollow display panel and a bottom-tethered photothermally responsive fluorescent actuator. Under NIR light, the photomechanically bending movements of the fluorescent actuator will immediately cover the hollow window of the display panel and synchronously manifest as the display of fluorescent patterns. Owing to its desirable time- and light-power-dependent actuating behaviors, diverse fluorescent patterns/information can be dynamically and reversibly displayed by facilely controlling this single remote NIR signal. This bioinspired strategy is universal and promising for fabricating on-demand fluorescent display platforms that combine a wide choice of fluorophores, remote control with high spatial/temporal precision, and especially single-input multiple-output features.

1. Introduction

Soft intelligent luminescent material systems,[1] which can behave like cephalopod skins to enable the on-demand display of dynamic colorful patterns/information upon stimulation,[2] have gained increasing popularity in diverse applications such as bioimaging probes,[3] information encryption,[4] stretchable electronics,[5] and dynamic camouflage.[6] To produce such systems, the most frequently reported strategy relied on the stimuli-responsive manipulation of either the covalent chemical structure transformations (e.g., ring-opening reaction of spiropyrane and E-isomer to Z-isomer configuration change of hydroxyl distyrylpyridine)[7] or noncovalent molecular packing/intramolecular motion changes of the incorporated fluorophores.[8] Consequently, their fluorescent outputs were spatially and/or temporally adjusted in response to external environmental changes, resulting in the display of many expected luminescent patterns/information.[9] However, this classic strategy is often limited to a few types of delicately designed luminescent molecules with elaborately synthesized fluorophores (e.g., spiropyrane derivatives or distyrylpyridine dyes). Moreover, it remains very challenging to achieve the reversible and rapid switch between multiple expected patterns by using one single soft intelligent fluorescent system. Such limited patterning display capacity is thus far inferior to that of the natural cephalopod skins. This might be due to the fact that these artificial display systems primarily relied on the stimuli-responsive chemical actions (e.g., molecular structure/conformation changes) to alter their optical outputs. But there are very few synthetic materials that have the integrated properties of reversibly/rapidly switched multicolor fluorescence and spatially/temporally controlled structure/conformation changes.

In contrast, cephalopods offer a drastically different display mechanism to efficiently switch between diverse skin color/patterns upon external environmental changes.[10] They have evolved to undergo quick transformation of skin color/patterns in the face of danger so as to disguise themselves from

H. Shi, S. Wu, M. Si, S. Wei, G. Lin, H. Liu, W. Lu, T. Chen
Key Laboratory of Marine Materials and Related Technologies
Zhejiang Key Laboratory of Marine Materials and Protective Technologies
Ningbo Institute of Materials Technology and Engineering
Chinese Academy of Sciences
Ningbo 315201, China
E-mail: luwei@nimte.ac.cn; tao.chen@nimte.ac.cn
H. Shi, S. Wu, M. Si, S. Wei, H. Liu, W. Lu, T. Chen
School of Chemical Sciences
University of Chinese Academy of Sciences
19A Yuquan Road, Beijing 100049, China
W. Xie
Public Technology Service Center
Ningbo Institute of Materials Technology and Engineering
Chinese Academy of Sciences
Ningbo 315201, China
The ORCID identification number(s) for the author(s) of this article can be found under https://doi.org/10.1002/adma.202107452.

DOI: 10.1002/adma.202107452

predators. The coloration process has been reported to rely on the skin chromatophores composed of pigment granules that are attached to radial muscle fibers. Their skin colors/patterns are then mediated by nerve impulse (bioelectricity) controlled muscle contracting and releasing movements toward stimulation, which immediately convert to mechanical contraction and expansion of skin chromatophores, and finally manifest as body color/pattern changes.[11] Obviously, this natural display process primarily depends on the stimuli-responsive mechanical actions, that is, bioelectromechanically modulated patterning display strategy. In other words, this is a S → M → O cascading process, where S denotes the bioelectricity stimulation, M corresponds to mechanical movement, and O denotes the optical outputs. Such natural cascading behaviors have been made good use of and given out appealing achievements for constructing wonderful artificial homeostatic systems and chemomechanical sorting systems.[12] These elegant successes inspired us to believe that, if such natural patterning display tactic was implemented and replicated, it would significantly advance the design of artificial luminescent display systems. It is anticipated that such bioinspired mechanically modulated display system may not only enable the remote control of fluorescent outputs with spatial/temporal precision, but also make it possible to allow the stimuli-triggered rapid and reversible switching between various multicolor fluorescent patterns (the desirable single-input multiple-output feature) through well-tunable mechanical action. Meanwhile, such a novel "S → M → O" strategy is believed to allow a wide choice of stimuli-responsive polymers for actuation and chromophores for coloration.[13]

To prove this hypothesis, we herein draw inspiration from the bioelectromechanical display mechanism of cephalopods to develop a conceptually new photomechanically modulated fluorescent system, which enables on-demand display of fluorescent patterns via an NIR-light-regulated actuating process. Its design architecture and working principle are illustrated in **Scheme 1**. This biomimetic system consists of two main components, that is, one top suspended display panel with a hollow window ("displayer") and one NIR-light-controlled trilayer fluorescent actuator tethered beneath (Scheme 1a). The fluorescent actuator was prepared by layer-by-layer composition of the fluorescent glycol gel film, poly(dimethylsiloxane) (PDMS) thin film and carbon nanotubes (CNTs) film, aiming at mimicking the function of skin chromatophores in cephalopods (Scheme 1b). Specifically, the CNTs film layer served as a signal "processor" that can efficiently transform the input NIR-light stimuli to conductible heat flux owing to its excellent photothermal conversion capability in NIR window. When the heat was transferred to the PDMS layer with high thermal expansion coefficient, this trilayer actuator ("effector") spontaneously deformed toward the fluorescent gel layer to cover the hollow window of the "displayer" (Scheme 1c). As a result, dynamic fluorescent patterns or information were observed on the display panel (Scheme 1d,e). By utilizing customized display panels, diverse desirable fluorescent patterns or information could be dynamically displayed on our photomechanically modulated system by remotely regulating the NIR-light power, suggesting its remote control and desirable "single-input, multioutput" features. Based on synergistic effect of these appealing properties, their potential applications for dynamic paintings/figures and high-level information encryption were further demonstrated.

2. Results and Discussion

2.1. Preparation of the Lanthanide Coordinated Supramolecular Multicolor Fluorescent Glycol Gels (PHM6A-Eu/Tb)

In this study, we aimed to realize the on-demand display of colorful fluorescent patterns. For this purpose, multicolor fluorescent polymer gel materials with self-healing feature were designed and prepared in the first place. **Figure 1**a depicts their synthetic procedures. Briefly, thermally induced free radical copolymerization of potassium 6-acrylamidopicolinate (K6APA), methyl 6-(3-(2-(methacryloyloxy)ethyl)ureido)picolinate (MAUP) and *N*-(2-hydroxyethyl) acrylamide (HEAA) was first conducted in dimethyl sulfoxide (DMSO) to synthesize poly(HEAA-MAUP-K6APA), abbreviated as PHM6A. The obtained DMSO gels were then treated in excess glycol solutions of Eu^{3+}/Tb^{3+} ions to produce PHM6A-Eu/Tb gels with both red and green fluorescent centers. In the absence of chemical crosslinkers, their dynamic polymer networks were constructed totally by noncovalent interactions.

For one, robust multiple hydrogen bonding was mainly contributed by the moieties of MAUP, which was evidenced by in situ Fourier transform infrared (FT-IR) spectroscopy (Figure 1b). With temperature increasing from 20 to 100 °C, the stretching vibration peak of C=O bond (≈1652 cm^{-1}) in ureido blueshifted while the bending vibration peak of N—H bond (≈1558 cm^{-1}) in ureido redshifted, signifying the dissociation of hydrogen bonds.[14] To further testify the role of multiple hydrogen bonding, atomic force microscopy (AFM) measurements were performed to compare the Young's modulus distribution of PHM6A gel before and after treatment to trifluoroacetic acid (TFA) (Figure S1, Supporting Information).[15] As TFA could break the dimers of ureido-picolinate and induce the decrease of hydrogen bonding density, TFA-treated PHM6A gel suffered a significant reduction in both mean Young's modulus and mean surface roughness.

For another, dynamic lanthanide-coordinated crosslinks were mainly formed between K6APA and lanthanide ions (Eu^{3+} or Tb^{3+}) and investigated by X-ray photoelectron spectroscopy (XPS). Through fitting analysis, the Eu3d binding energies of PHM6A-Eu gel were assinged to $3d_{3/2}$ (1162.2 eV) and $3d_{5/2}$ (1132.1 eV) of excess free Eu^{3+}, as well as $3d_{3/2}$ (1151.6 eV) and $3d_{5/2}$ (1122.1 eV) of bonded Eu atoms that shared electron pairs with N atoms in pyridine or O atoms in —COO— (Figure 1c). Similar shifts toward lower binding energy were observed for the Eu4d spectra of PHM6A-Eu gel and Tb4d spectra of PHM6A-Tb gel (Figure S2, Supporting Information) due to the increase of electron density, revealing the formation of lanthanide ion-ligand coordination. The obviously enhanced mechanical properties of PHM6A-Eu and PHM6A-Tb samples further demonstrated the formation of lanthanide coordinated crosslinks (Figure S3, Supporting Information). Besides, the results of elemental mapping by energy-dispersive X-ray spectroscopy (EDS) indicated the even distribution of these fluorescent K6APA-Eu/Tb complexes in the PHM6A-Eu/Tb gels

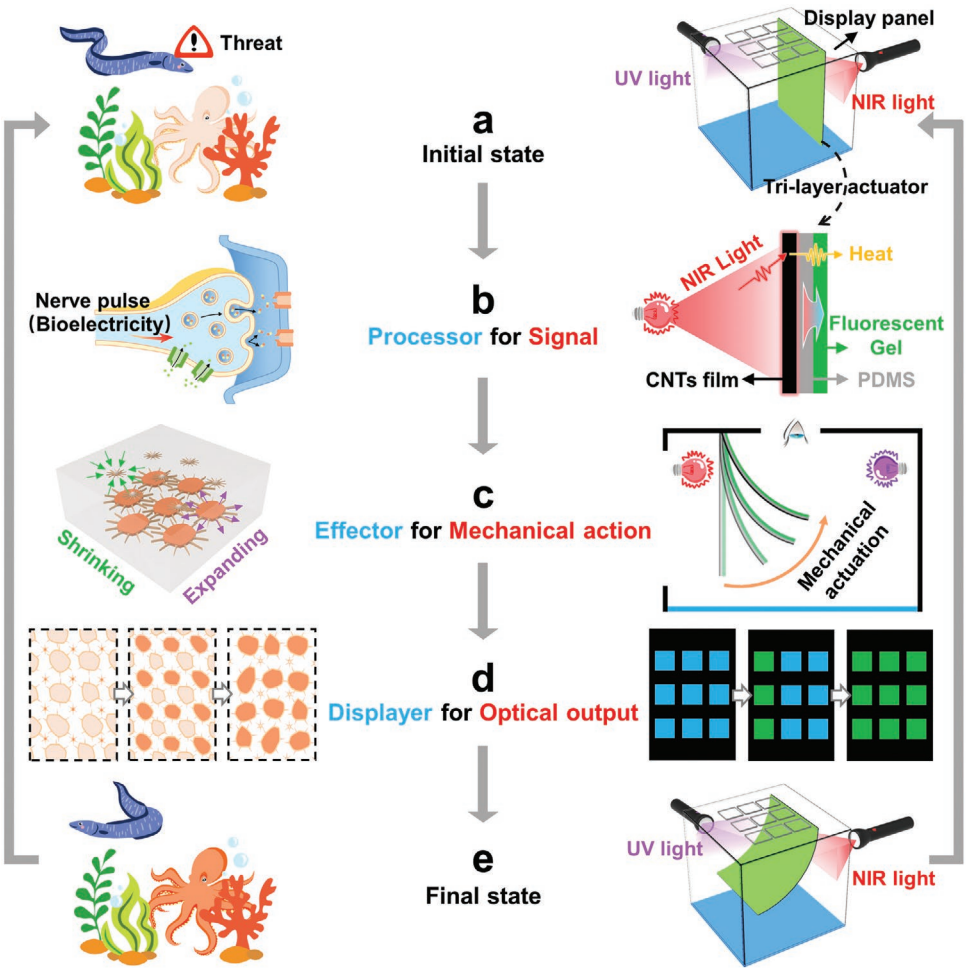

Scheme 1. Illustration of the biological inspiration (left) and the photomechanically modulated display system design (right). a) Initial state. Cephalopod in face of predator and biomimetic system exposed to NIR light. The exterior surface of the biomimetic system is black and opaque in fact, but set as transparent herein to demonstrate interior and rear arrangement. b) Processor for signal. Conversion of external stimuli to bioelectricity by neurons in the cephalopod and to heat flux by CNTs film in this biomimetic system. c) Effector for mechanical action. Shape deformation of skin chromatophores by muscle movements in the cephalopod and trilayer fluorescent actuator by PDMS expansion in the biomimetic system. d) Displayer for optical outputs. Cephalopod skin pattern change and the displayed fluorescent pattern change on the biomimetic system. e) Final state. Cephalopod realizing concealment from a predator and biomimetic system finishing on-demand fluorescent patterning.

(Figure 1d), clearly suggesting the quite good homogeneity of the material structures and properties. In particular, from the results of UV absorption spectra (Figure S4a,b, Supporting Information), coordination between lanthanide ions and MAUP was negligible. This was because the competitive effect among K6APA, MAUP and glycol, where such lanthanide ions as Eu^{3+} and Tb^{3+} showed sequentially diminished affinity to O atoms in $-COO^-$ of K6APA, −OH of glycol and C=O of MAUP according to hard–soft–acid–base theory. Therefore, the formation of MAUP-Eu^{3+}/Tb^{3+} coordination bonds were significantly suppressed by plenty of glycol molecules in the polymeric network, while the binding of K6APA and Eu^{3+}/Tb^{3+} was robust and unaffected.

Optical properties of the as-prepared fluorescent polymer gels were then studied. Though the PHM6A and PHM6A-Eu/Tb gels looked highly transparent under visible light (Figure S5, Supporting Information), their UV absorption (Figure S4c, Supporting Information) and fluorescent spectra (Figure S6, Supporting Information) turned out to be quite different. It was because pyridine carboxylate groups could serve as good sensitizers for lanthanide ions and significantly increase their emission intensities through a well-known resonance energy transfer process.[16] To be specific, under 245 nm UV irradiation, PHM6A-Eu and PHM6A-Tb gels gave out bright red and green fluorescence, respectively. PHM6A-Eu/Tb gels with a variety of fluorescence colors could be further prepared by treating the as-prepared PHM6A gels in the Eu^{3+}/Tb^{3+} mixtures of different molar ratio. As suggested by Figure 1e,f, with increasing Tb^{3+}/Eu^{3+}, the emission intensity ratio of green band at 547 nm to red band at 617 nm gradually increased, resulting in the overlapping fluorescent color change. Therefore, responsive fluorescence color changes from green to yellow and even red were further realized by exposing the PHM6A-Tb gel to the Eu^{3+} stimulus, and vice versa if exposing the PHM6A-Eu gel to the Tb^{3+} stimulus (Figure S7, Supporting Information). On the other hand, upon exposure to HCl/NH_3 vapor, responsive

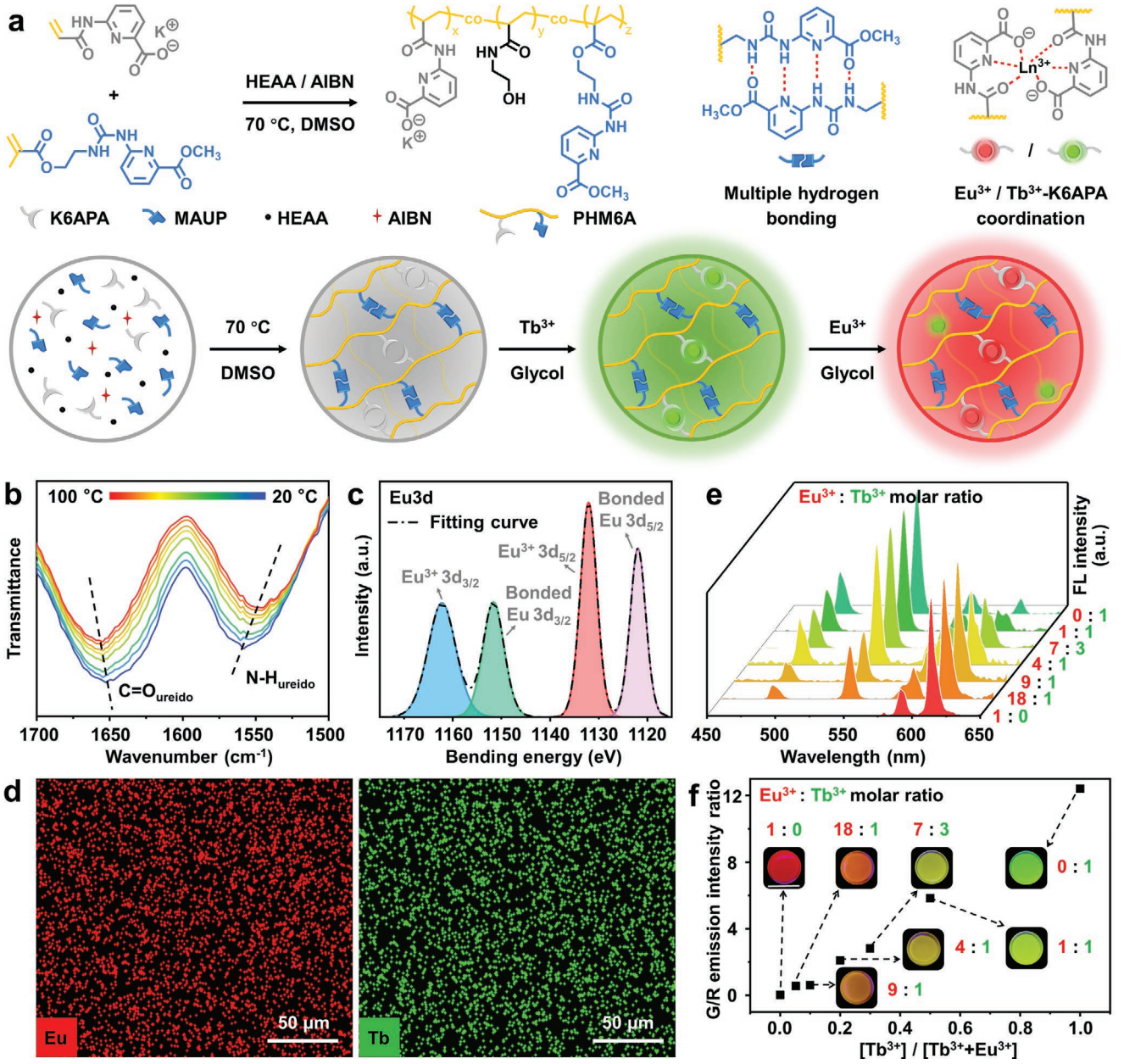

Figure 1. Fabrication and characterization of multicolor fluorescent PHM6A-Eu/Tb gels. a) Illustration showing the synthesis of PHM6A-Eu/Tb gels and the chemical structures. b) FT-IR spectra of PHM6A with temperature increasing from 20 to 100 °C at an interval of 10 °C. c) High-resolution XPS fitting results for Eu3d spectra of PHM6A-Eu. d) EDS mapping of Eu in PHM6A-Eu gel (left) and Tb in PHM6A-Tb gel (right). e) Fluorescence spectra (λ_{ex} = 254 nm) of PHM6A-Eu/Tb gels with different Eu^{3+}/Tb^{3+} molar ratio. f) The green/red emission intensity ratio (547 nm vs 617 nm) as a function of the Eu^{3+}/Tb^{3+} molar ratio and corresponding photos taken under a 254 nm UV lamp. The scale bars in all the digital photos are 1 cm.

fluorescence quenching/recovery took place for both PHM6A-Eu and PHM6A-Tb gels and were verified by 3D fluorescence spectra (Figure S8, Supporting Information). This could be explained by the pH-controlled dissociation and reformation of these fluorescent K6APA-Eu/Tb complexes.

What's more, due to the presence of multiple hydrogen bonding crosslinks, the supramolecular fluorescent gel is inherent with a degree of self-healing capacity (Figure S9a, Supporting Information). Taking advantage of the multiple fluorescence colors of PHM6A-Eu/Tb gel synergistically, complex fluorescent pattern would be facilely constructed by healing several separate gels into one piece. For example, a 3D color code was prepared after forcing proper gels to self-heal at 60 °C for 4 h, which could then serve as a useful tool for information encryption (Figure S9b, Supporting Information). Thus, PHM6A-Eu/Tb gel with both tunable multifluorescence-color and self-healing capacity is expected to be a novel kind of fluorescent materials promising for various applications.

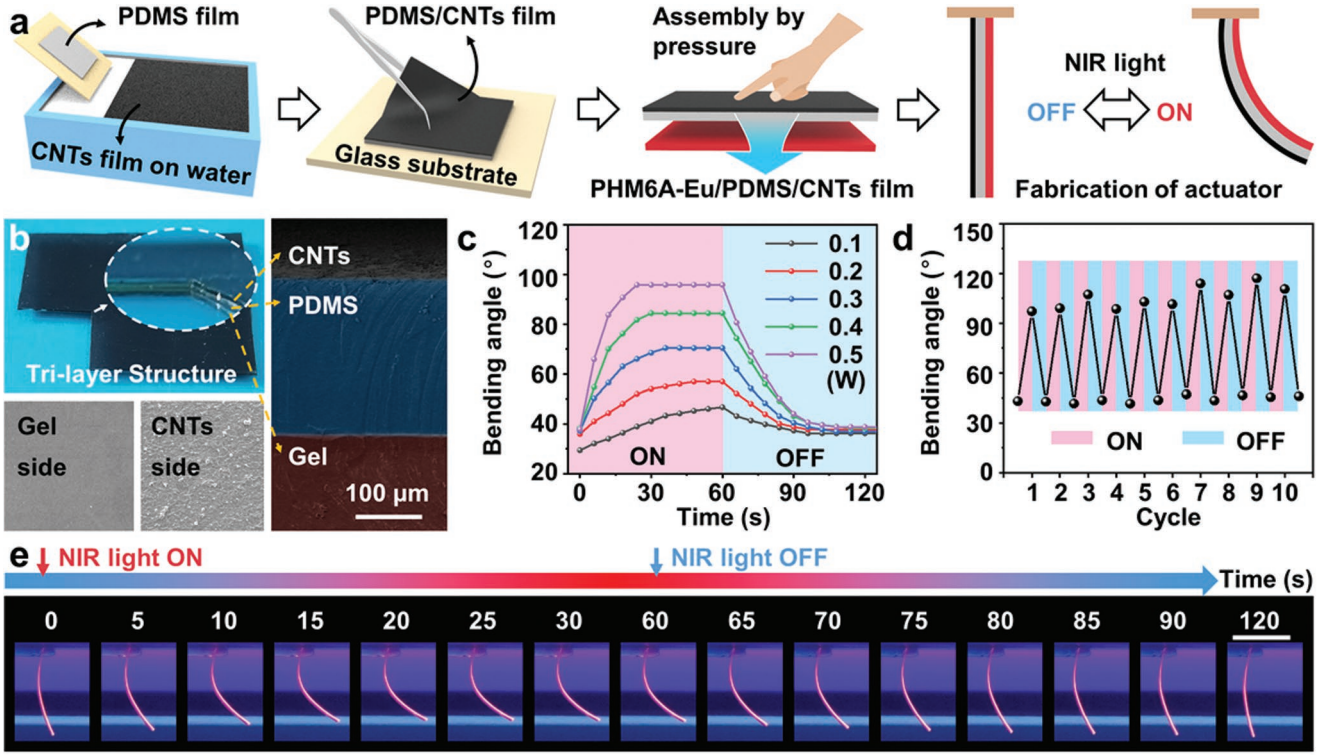

Figure 2. Fabrication and characterization of trilayer fluorescent PHM6A-Eu/PDMS/CNTs actuator. a) Illustration showing the step-by-step preparation of a trilayer fluorescent actuator comprising condensed CNTs film, PDMS and PHM6A-Eu gel film. b) Photograph, cross-section SEM image (colored), and surface SEM images (gray) of the actuator. c) Bending angle of the actuator as a function of time when it was exposed to NIR light with different powers (0.1–0.5 W). d) Cyclic actuation process of the actuator by turning on/off NIR light (0.5 W). e) Photos showing continuous shape deformation and recovery process of the actuator triggered by NIR light (0.5 W). The scale bars in all the digital photos are 1 cm.

2.2. Fabrication of the Trilayer Fluorescent Actuators (PHM6A-Eu/PDMS/CNTs)

Having obtained the multicolor fluorescent polymer gels, the actuators were then fabricated by a layer-by-layer composition of the condensed CNTs film, PDMS and PHM6A-Eu/Tb gel film. Condensed CNTs film was generated on the surface of water by a Marangoni spread and capillary force induced compression of multiwall CNTs according to the reported method (**Figure 2**a).[17] Subsequently, the commercial PDMS film with a thickness of 200 μm was used to transfer the CNTs film to produce the PDMS/CNTs bilayer film that were closely bonded together by hydrophobic effect. Owing to excellent photothermal conversion capability of the condensed CNTs film, the as-prepared bilayer film (0.5 cm × 0.5 cm) was found to exhibit a rapid temperature increase to a plateau within 25 s under 808 nm NIR irradiation (Figures S10 and S11a, Supporting Information). The maximum temperatures of the material exhibited positive correlation with the NIR-light power (Figure S11b, Supporting Information). For example, upon increasing the NIR-light power from 0.1 to 0.5 W, their maximum temperature increased from less than 50 °C to more than 80 °C, suggesting the wide temperature tunability. When the NIR light was turned off, a sharp decline of temperature down to room temperature occurred within 30 s. These results indicated the quick photothermal conversion rate as well as the cooling rate of the PDMS/CNTs bilayer film, which is essential to achieve the elegant control of the following actuating behaviors.

Later, the as-prepared PDMS/CNTs bilayer film was pressed together with the fluorescent PHM6A-Eu gel film at room temperature to fabricate the trilayer fluorescent PHM6A-Eu/PDMS/CNTs actuator. To ensure their stable interfacial composition, the glycol gel was first pretreated in an oven at 70 °C for 24 h to remove partial solvent and afford the thin PHM6A-Eu gel film, which had a thickness of 150 μm or so and a glycol content of 37.5 wt% on average (Table S1, Supporting Information). The trilayer interfacial structure of the fluorescent actuator could be clearly observed by scanning electron microscopy (SEM) (Figure 2b) and polarizing microscopy (Figure S12, Supporting Information), indicating that these layers were tightly combined without gaps. Both surfaces of the anisotropic actuator were also characterized by SEM, which showed that the gel side appeared to be smooth and the CNTs side appeared to be coarse.

Actuation behavior of the straight PHM6A-Eu/PDMS/CNTs actuator (1.8 cm × 0.5 cm) was then tested with one end tethered. Upon exposure to NIR irradiation, the generated heat of CNTs film layer was spontaneously transferred to the adjacent PDMS layer. The instant thermal expansion of PDMS layer forced this straight actuator to bend toward the fluorescent gel layer. It is worth noting that the fluorescent gel layer was proved to be indispensable, as was evidenced by the control experiment that no actuating behavior was observed for the PDMS/CNTs

bilayer film (Figure S13, Supporting Information). For PDMS/CNTs bilayer film, the influence from the thermal expansion of PDMS could be eliminated by the flexible stretching of the closely packed CNTs film. Nevertheless, since fluorescent gel layer possessed higher tensile resistance, the mismatch between PDMS and gel at high temperature had to be settled by a distinct bending deformation, which accounted for the responsiveness of the trilayer fluorescent actuator. Importantly, the actuating behaviors of our PHM6A-Eu/PDMS/CNTs actuator could be facilely regulated by varying the NIR-light power. As summarized in Figure 2c, higher-power NIR light was found to trigger faster actuating rate, larger bending angle (θ) and earlier equilibrium period, because the thermal expansion extent of PDMS layer was largely temperature-dependent. After turning off the NIR light, the actuator cooled down to ambient temperature and recovered to the initial state in 1 min. The light-triggered actuating process was demonstrated to be reversible and could be held for at least ten cycles (Figure 2d,e), laying a solid foundation for the following displaying use.

2.3. The Photomechanically Modulated Fluorescent Systems for On-Demand Display of Fluorescent Patterns

Inspired from the cascading S → M → O display strategy of cephalopods, a mechanically modulated fluorescent system was constructed. Its general, customizable design is presented in **Figure 3**a and its real image is shown in Figure S14 in the Supporting Information. One end of the red fluorescent PHM6A-Eu/PDMS/CNTs actuator was tethered onto the top suspended display panel with a hollow window, while the bottom background substrate with static blue fluorescence was made of

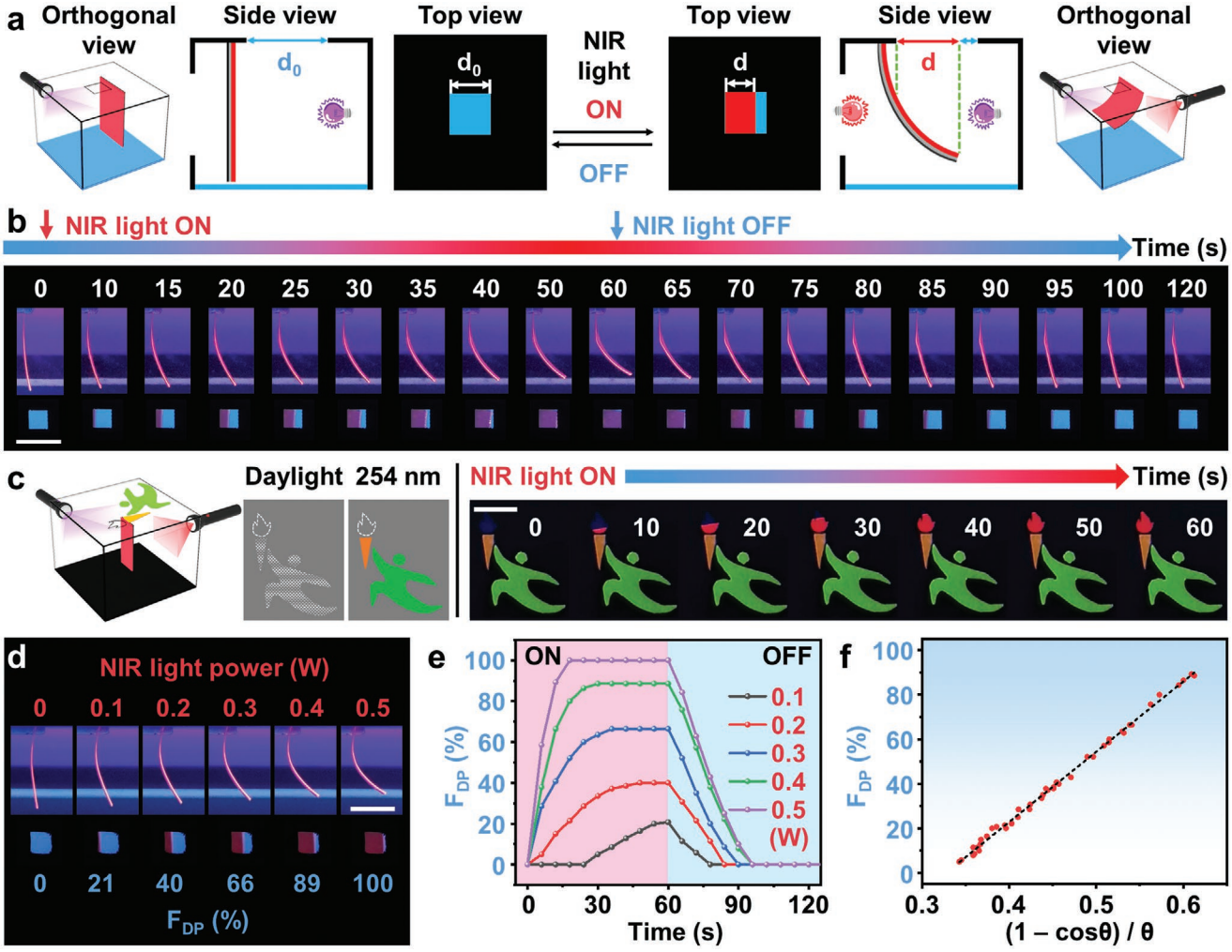

Figure 3. Construction of photomechanically modulated fluorescent system. a) Illustration showing the architecture of the system and the mechanism of dynamic fluorescent patterning on the top display panel. b) Photos showing continuous shape deformation and recovery process of the trilayer fluorescent actuator (top) as well as corresponding fluorescence change of the square pattern (bottom) triggered by NIR light (0.5 W). c) Schemes and photos showing the dynamic display of a fluorescent painting named as "a torchbearer" by applying NIR light (0.5 W). d) Photos showing different actuating behaviors and optical outputs of the system under different NIR-light power (0–0.5 W). e) The fluorescence displacement percentage (F_{DP}) as a function of time when the actuator is exposed to NIR light with different powers (0.1–0.5 W). F_{DP} was defined as d/d_0, where d_0 was the length of the hollow window and d was the length of the newly appearing red fluorescent part. f) Fitting results of F_{DP} versus bending angle-related parameter $(1 - \cos\theta)/\theta$. The scale bars in all the digital photos are 1 cm.

N-vinyl carbazole (NVC)-loaded filter paper. When there was no NIR irradiation, the actuator was in upright state, leaving the top panel to display the static blue fluorescence of bottom background. Upon NIR irradiation (0.5 W), the tethered actuator gradually deformed to partially cover the open window of the top display panel. As a result, dynamically changed fluorescent patterns were observed. As shown in Figure 3b, the bending angle of the actuator increased over time, and accordingly, the percentage of red fluorescence increased at the cost of decreasing blue fluorescence. On account of the reversibility of the actuator, the new pattern could be switched back to its initial state once the NIR light was withdrawn. Such an ability to achieve the fast and reversible switching between many different fluorescent patterns in response to NIR-light stimuli is of fundamental interest and has seldom been reported previously.

By using this bioinspired photomechanically modulated fluorescent system, many desirable fluorescent patterns could be dynamically displayed as long as the customized display panels were utilized. As an example, one typical display panel was designed and illustrated in Figure 3c, in which the green man and yellow torch was made from PHM6A-Tb gel and PHM6A-Tb/Eu gel, respectively. Note that the flame part in the display panel was hollow, but one red fluorescent PHM6A-Eu/PDMS/CNTs actuator was tethered below it. At the initial state, only a green man lifting a yellow torch with no flame was observed on the display panel. Once NIR light was applied, the red fluorescent actuator would bend to cover the hollow flame and thus enable the gradual appearance of red flame. Consequently, the whole image of a green man lifting a flaming torch was displayed through remote control of NIR light. More importantly, on the basis of the same display system, it was possible to produce diverse fluorescent patterns such as the dynamic 3D color code (Figure S15, Supporting Information), apple tree image (Figure S16, Supporting Information) and so on by merely utilizing different display panels. These results clearly demonstrated their powerful "single-input, multiple-output" features.

Besides time dependence, it was further found that the NIR-triggered bending behaviors of the red fluorescent PHM6A-Eu/PDMS/CNTs actuator were largely dependent on the power of NIR light. Figure 3d depicts its actuating photos under different NIR-light power (0–0.5 W). For the convenience of quantitative description, the fluorescence displacement percentage (F_{DP}) was defined as d/d_0, where d_0 was the length of the hollow window and d was the length of the newly appearing red fluorescent part. As summarized in Figure 3e, the F_{DP} values showed positive correlation with the NIR-light power at given irradiation time. For example, under 0.5 W NIR light, F_{DP} rose quickly to 100% within 15 s, but in the case of 0.2 W NIR light, F_{DP} increased slowly and stabilize at around 40% even after 1 min. According to model analysis (Note S1 and Figure S17, Supporting Information), the F_{DP} should be linearly correlated with bending angle-related parameter $(1 - \cos\theta)/\theta$ at ideal conditions, which was testified by fitting data points measured from experiment (Figure 3f). This quantitative relationship was helpful to guide the precise control of the displayed fluorescent patterns. Similar to the red fluorescent PHM6A-Eu/PDMS/CNTs actuator, the NIR light power dependent actuating behaviors were observed for the green fluorescent PHM6A-Tb/PDMS/CNTs actuator as well (Figure S18, Supporting Information). This finding suggested the possibility to achieve on-demand display of more complex fluorescent patterns by remotely varying the NIR-light power, which was of fundamental importance for many potential high-tech applications, including dynamic paintings/figures, information encryption.

Next, we explored to utilize the NIR light power dependent actuating behaviors of the photomechanically modulated fluorescent systems to showcase their potential application for the on-demand display of a dynamic painting named as "growing seedling." To this end, a display panel loaded with one yellow mound-like PHM6A-Tb/Eu gel and one seedling-like hollow region was designed. A green fluorescent PHM6A-Tb/PDMS/CNTs actuator was tethered below the hollow region (**Figure 4**a). When there was no NIR irradiation, only a yellow mound was displayed at the initial state (Figure 4b). As expected, under NIR irradiation, the green fluorescent PHM6A-Tb/PDMS/CNTs actuator gradually bent to cover the hollow seedling window. Correspondingly, the "growing seedling" figure was dynamically displayed, in which a green seedling slowly sprouted out from the mound and came into leaf over time. Remarkably, quite different final outputs of the system after applying NIR light for 1 min could be acquired by facilely varying the NIR-light power, ranging from a seedling that just broke ground to that grew up with one or two leaves (Figure 4b). In this way, by using this specially designed photomechanically modulated fluorescent system, on-demand display of dynamic paintings was successfully demonstrated by simply varying one single remote NIR signal, which has never been achieved by using the conventional chemically responsive fluorescent materials.

Besides, high security data encryption and on-demand decryption was realized by utilizing a top suspended display panel that was hollowed-out with a pattern of "8." As schemed in Figure 4c, in the absence of NIR light, the green fluorescent PHM6A-Tb/PDMS/CNTs actuator was in upright state and thus no information was displayed. By applying a low-power (0.2 W) NIR light for 1 min, the tethered actuator deformed to partially cover the hollow region, enabling the display of a green fluorescent number "1" on the panel. As the F_{DP} tended to be larger when the actuator was exposed to medium-power (0.5 W) or high-power (0.8 W) NIR light, different information would be decrypted, which manifested as number "3" and "8," respectively.

To further enhance encoding complexity, the multicolor characteristics of the fluorescent gel layer were capitalized on for colorful fluorescent pattern display and information encryption. To do this, different parts of the gel layer was first converted to be yellow, green, and red fluorescent by Tb^{3+}/Eu^{3+}, Tb^{3+}, and Eu^{3+} ion printing respectively according to the reported methods.[8d] As illustrated in Figure 4d, such a tricolor fluorescent actuator was then tethered below a well-designed display panel, on which the patterns of a blossom, two leaves and a pot was hollow. As expected, no fluorescent pattern was observed on the display panel without NIR irradiation. When low-power (0.5 W) NIR light was applied, small deformation of the actuator enabled its anterior red fluorescence to exactly cover the hollow pot. At the moment, only a red pot was displayed on the top panel. Yet, medium-power (1 W) NIR light would bring about larger deformation of the actuator, and make its anterior red fluorescence as well as middle green fluorescence appear

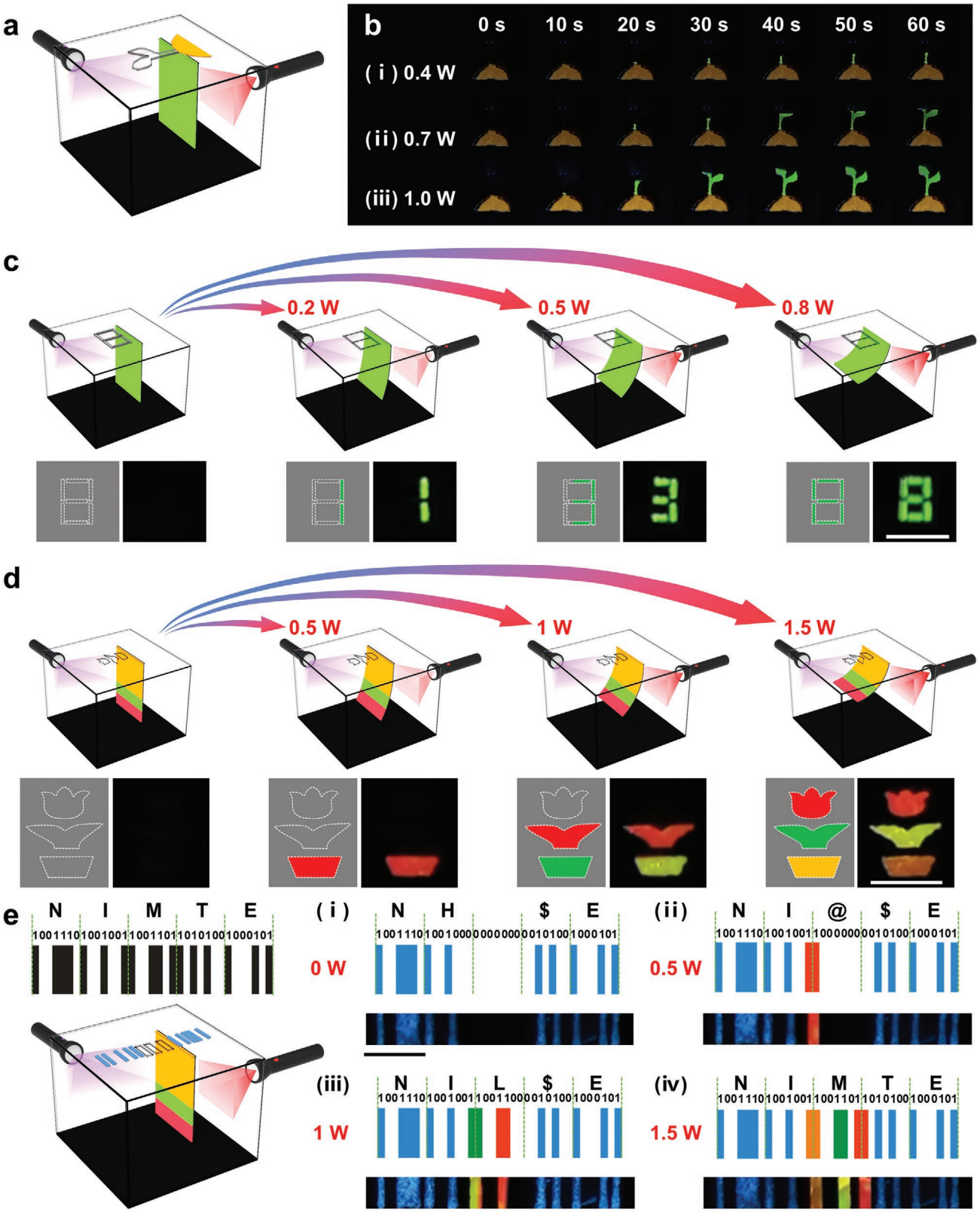

Figure 4. On-demand display of diverse fluorescent patterns for dynamic paintings/figures and information encryption applications. a,b) Scheme of the system and the photos showing on-demand display of a dynamic painting named as "growing seedling" by varying NIR-light power. c–e) Schemes of the systems and the corresponding photos showing on-demand display of the fluorescent number, a potted plant and 2D barcode by facilely varying the NIR-light power. The scale bars in all the digital photos are 1 cm.

beneath the hollow pot and leaves respectively, presenting as a picture of red leaves in a green pot on the display panel. Furthermore, major deformation of the actuator occurred on the condition of high-power (1.5 W) NIR light, so that its anterior red fluorescence, middle green fluorescence and posterior yellow fluorescence could simultaneously cover the hollow blossom, leaves and pot respectively, which generated a new picture with red blossom, green leaves and yellow pot. Such colorful fluorescent pattern display process was also capable of being reversed (Figure S19, Supporting Information).

Using a similar approach, dynamic barcode labels for the anticounterfeiting applications were envisioned. As Figure 4e showed, incomplete blue florescent barcode was printed onto the display panel beforehand, while the rest part of barcode was set to be hollow. In this design, the length of the whole barcode was 5×7 units. The fluorescent and nonfluorescent state of each unit were defined as "1" and "0," respectively. Every seven units comprised one binary code that corresponded to a specific character on the basis of standard ASCII codes. At the initial state, only a barcode in blue was observed, which could be translated to a character string "NH $E." When low- (0.5 W), medium- (1 W), and high-power (1.5 W) NIR light was applied, different deformation extents of the tricolor fluorescent actuator contributed to the reversible display of bi-, tri-, and tetracolored barcode on the panel, respectively (Figure S20, Supporting Information). Consequently, various information in the meaning of "NI@$E," "NIL$E," and "NIMTE" respectively was decoded. These results indicated that the distinctive ability of our photomechanical system for on-demand display of different fluorescent patterns. Such a powerful data encryption platform could largely improve the data security level because different information would be decrypted by facilely varying the NIR-light power.

3. Conclusion

We have drawn inspiration from the cascading S → M → O display strategy of cephalopods to develop a conceptually new photomechanically modulated fluorescent system. Its key component is a trilayer fluorescent actuator consisting of the fluorescent PHM6A-Tb/Eu gel film, PDMS and CNTs films. When paired with certain customizable display panel, the NIR-light-triggered mechanical deformation of the actuator would convert to synchronous fluorescence displacement in the hollow region and hence generate a time-dependent optical output from the system. Besides, given that the actuating behaviors of the actuator could be facilely tailored by varying NIR-light power, the optical output also featured NIR-light power dependence, which was verified by the experimental observation. Taking advantage of these characteristics, several interesting prototypes (e.g., variable pictures and information codes) for dynamic painting and high security information encryption applications were further demonstrated by facilely varying this single remote NIR input signal.

The bioinspired photomechanically modulated display mechanism is the key novelty of the present system, in contrast with most of the reported dynamic fluorescent systems that primarily depend on the stimuli-responsive chemical actions to alter their optical outputs. As demonstrated in this study, such a bioinspired design offered many unique advantages, including remote control with spatial/temporal precision, single-input multiple-output, as well as a wide choice of fluorophores. These desirable advantages are highly appealing but have never been realized previously on one single smart fluorescent display system. The success of this biomimetic system was expected to be a starting point for the exploration of more potent fluorescent display applications and may inspire better materials, stimulations and display strategies for future research.

4. Experimental Section

Materials: *N*-(2-hydroxyethyl)acrylamide (HEAA, 98%, stabilized with 4-methoxyphenol) was purchased from Shanghai Macklin Biochemical Co. Ltd. 2,2′-azoisobutyronitrile (AIBN, 99%) were provided by J&K Scientific Ltd. $Eu(NO_3)_3 \cdot 6H_2O$ (99.9%) and potassium hydroxide (KOH, 95.0%) were supplied by Energy Chemical. $Tb(NO_3)_3 \cdot 5H_2O$ (99.9%), trifluoromethanesulfonic acid (TFA, 99%), and NVC (98%) were purchased from Aladdin Chemistry Co. Ltd. DMSO (99%), glycol (99%), methanol (99%), ethanol (99%), hydrochloric acid (HCl, F.W. 36.46, 99%), ammonia solution (NH_3, F.W.17.03, 99%), and filter papers were obtained from Sinopharm Chemical Reagent Co. Ltd. The raw carbon nanotubes (CNTs) (diameter, about 8–15 nm; length, about 50 μm; —COOH%, about 1.23 wt%) with purity of over 98% were gotten from Chengdu Organic Chemistry Co., Ltd. PDMS films (250 mm × 200 mm × 200 μm) were purchased from Hangzhou Bald Advanced Materials Co. Ltd. HEAA passed through an alumina column to remove stabilizer before use. AIBN was purified through recrystallization and vacuum distillation. Other materials were used as received. Monomers methyl MAUP and 6-acrylamidopicolinic acid (6APA) were synthesized according to the procedures described in the previous study.[6a,17]

Fabrication of Multicolor Fluorescent Glycol Gel Films: Monomers HEAA (2.45 g, 21.3 mmol), MAUP (0.35 g, 1.14 mmol), 6APA (0.14 g, 0.73 mmol), and initiator AIBN (8 mg, 0.049 mmol) were dissolved in DMSO (10 mL) and then mixed with 82 μL KOH aqueous solution (0.5 g mL^{-1}, 0.73 mmol). The precursor solution was added into the mold with two quartz glass plates and a 1 mm thick silicon plate, followed by free radical copolymerization at 70 °C for 10 h to prepare the PHM6A gels. Subsequently, the PHM6A gels were immersed in excess glycol solution of Eu^{3+}/Tb^{3+} (1 M) for 2 h and rinsed in glycol for 4 h to obtain fluorescent PHM6A-Eu/Tb gels. Finally, most of the solvent in PHM6A-Eu/Tb gels was evaporated at 70 °C for 24 h to afford multicolor fluorescent glycol gel films.

Fabrication of CNTs Film: The CNTs films were fabricated by the method according to the previous study.[17] First, the CNTs were mixed with ethanol (2 mg mL^{-1}) and dispersed by ultrasonication for 8 h. Then, a certain volume of the as-prepared dispersion was sprayed onto the water surface, resulting in a uniform and ultrathin CNTs-based film at the air/water interface. Later, a piece of microporous sponge was placed at the edge of the film to break the equilibrium the surface tension of the system, which induced the contraction of the preassembled film and the formation of a condensed CNTs film. The compression procedure was repeated until the CNTs film cannot be condensed further.

Fabrication of Bilayer PDMS/CNTs Film: PDMS cut into appropriate shape was conformally fixed on a glass substrate. Then the condensed CNTs film floating on air/water interface was transferred to the surface of PDMS using lift-up transferring method, followed by drying at room temperature for 12 h to obtain a flat bilayer PDMS/CNTs film.

Fabrication of Trilayer Fluorescent Actuator: Multicolor fluorescent glycol gel film was stuck to the PDMS side of the bilayer CNTs/PDMS film simply by pressing. A flat trilayer PHM6A-Eu/PDMS/CNTs or PHM6A-Tb/PDMS/CNTs film was produced and then cut into appropriate shape to fabricate trilayer fluorescent actuator.

Fabrication of Photomechanically Modulated Fluorescent System: A piece of black paper was cut into appropriate shape by a laser cutting machine, which could be folded into a black box. According to the

design requirements, the bottom of the box was selectively covered by fluorescent materials. The top of the box was set as display panel, whose partial region was designed to be hollow or covered by fluorescent materials. Then a trilayer fluorescent actuator was fixed to the interior of the box using foam tape. UV light (254 nm) and NIR light (808 nm) were introduced from two vertical directions to trigger fluorescence and shape deformation, respectively. Thereby, the system could display various fluorescent pattern on demand.

Characterization: The digital photos of the fluorescent materials were taken by smart phone camera (HUAWEI P40 Pro) under a UV lamp (ZF-5, 8 W, 254 nm). Temperature-dependent FT-IR spectra were recorded on Thermo Scientific Nicolet 6700 FT-IR spectrometer equipped with a temperature control module. AFM measurements were conducted using Dimension ICON SPM (Bruker, USA) in a PeakForce tapping mode. XPS characterization was performed on Kratos AXIS ULTRADLD instrument with a monochromic Al K_α X-ray source. Tensile test was conducted on Z1 Zwick/Roell Universal Testing System. UV–vis absorption and transmittance spectra were acquired from Perkin-Elmer LAMBDA 950 UV/Vis/NIR spectrophotometer. Hitachi F-4600 fluorescence spectrofluorometer with a 150 W Xenon lamp was used to measure fluorescence spectra. Surface EDS mapping and cross-section morphology of the samples were characterized by Hitachi S-4800 field-emission scanning electron microscopy. Microscopy images were obtained using an OLYMPUS BX51 polarizing microscope. An IR thermal camera (Optris PI 400) was employed to capture the real-time surface temperature and IR images of the samples. NIR light was provided by an NIR laser source (BWT Beijing, K808DAHFN-15.00 W, 808 nm) and the horizontal distance between the light and the actuators was fixed at 5 cm.

Supporting Information

Supporting Information is available from the Wiley Online Library or from the author.

Acknowledgements

This work was supported by the National Natural Science Foundation of China (Grant No. 52073297, 21774138, and 51773215), the Sino-German Mobility Program (M-0424), the Key Research Program of Frontier Sciences, Chinese Academy of Sciences (QYZDB-SSW-SLH036), the National Key Research and Development Program of China (2019YFC1606603), the Youth Innovation Promotion Association of Chinese Academy of Sciences (2019297) and K.C. Wong Education Foundation (GJTD-2019-13).

Conflict of Interest

The authors declare no conflict of interest.

Data Availability Statement

Research data are not shared.

Keywords

bioinspired materials, fluorescent patterning, photomechanically, single-input multiple-output, soft actuators

Received: September 18, 2021
Revised: October 14, 2021
Published online: November 26, 2021

[1] a) H. Wang, X. Ji, Z. Li, F. Huang, *Adv. Mater.* **2017**, *29*, 1606117; b) Y. Li, D. J. Young, X. J. Loh, *Mater. Chem. Front.* **2019**, *3*, 1489; c) Z. Li, X. Ji, H. Xie, B. Z. Tang, *Adv. Mater.* **2021**, *33*, 2100021; d) S. Wei, Z. Li, W. Lu, H. Liu, J. Zhang, T. Chen, B. Z. Tang, *Angew. Chem., Int. Ed.* **2021**, *60*, 8608; e) X. K. Ma, Y. Liu, *Acc. Chem. Res.* **2021**, *54*, 3403.

[2] a) Y. Cheng, J. Wang, Z. Qiu, X. Zheng, N. L. C. Leung, J. W. Y. Lam, B. Z. Tang, *Adv. Mater.* **2017**, *29*, 1703900; b) M. Yu, P. Zhang, B. P. Krishnan, H. Wang, Y. Gao, S. Chen, R. Zeng, J. Cui, J. Chen, *Adv. Funct. Mater.* **2018**, *28*, 1804759; c) Q. Guo, B. Huang, C. Lu, T. Zhou, G. Su, L. Jia, X. Zhang, *Mater. Horiz.* **2019**, *6*, 996; d) Z. Li, P. Liu, X. Ji, J. Gong, Y. Hu, W. Wu, X. Wang, H. Q. Peng, R. T. K. Kwok, J. W. Y. Lam, J. Lu, B. Z. Tang, *Adv. Mater.* **2020**, *32*, 1906493; e) W. Zhang, Y. M. Zhang, F. Xie, X. Jin, J. Li, G. Yang, C. Gu, Y. Wang, S. X. Zhang, *Adv. Mater.* **2020**, *32*, 2003121.

[3] Y. Chen, T. Ma, P. Liu, J. Ren, Y. Li, H. Jiang, L. Zhang, J. Zhu, *Small* **2020**, *16*, 2005667.

[4] a) H. Sun, S. Liu, W. Lin, K. Y. Zhang, W. Lv, X. Huang, F. Huo, H. Yang, G. Jenkins, Q. Zhao, W. Huang, *Nat. Commun.* **2014**, *5*, 3601; b) J. Andreasson, U. Pischel, *Chem. Soc. Rev.* **2018**, *47*, 2266; c) S. Lin, H. Sun, J. Qiao, X. Ding, J. Guo, *Adv. Opt. Mater.* **2020**, *8*, 2000107; d) X. Le, H. Shang, H. Yan, J. Zhang, W. Lu, M. Liu, L. Wang, G. Lu, Q. Xue, T. Chen, *Angew. Chem., Int. Ed.* **2021**, *60*, 3640.

[5] a) Q. Wang, G. R. Gossweiler, S. L. Craig, X. Zhao, *Nat. Commun.* **2014**, *5*, 4899; b) C. Larson, B. Peele, J. Li, S. Robinson, M. Totaro, L. Beccai, B. Mazzolai, R. Shepherd, *Science* **2016**, *351*, 1071.

[6] a) S. Wei, W. Lu, X. Le, C. Ma, H. Lin, B. Wu, J. Zhang, P. Theato, T. Chen, *Angew. Chem., Int. Ed.* **2019**, *58*, 16243; b) Y. Huang, H. K. Bisoyi, S. Huang, M. Wang, X. M. Chen, Z. Liu, H. Yang, Q. Li, *Angew. Chem., Int. Ed.* **2021**, *60*, 11247.

[7] a) F. D. Jochum, P. Theato, *Chem. Soc. Rev.* **2013**, *42*, 7468; b) D. Kim, J. E. Kwon, S. Y. Park, *Adv. Funct. Mater.* **2018**, *28*, 1706213; c) M. Li, Q. Zhang, Y.-N. Zhou, S. Zhu, *Prog. Polym. Sci.* **2018**, *79*, 26; d) M. Xie, F. Xu, L. Zhang, J. Yin, X. Jiang, *ACS Macro Lett.* **2018**, *7*, 540; e) J. Ji, D. Hu, J. Yuan, Y. Wei, *Adv. Mater.* **2020**, *32*, 2004616; f) T. Li, K. Hu, X. Ma, W. Zhang, J. Yin, X. Jiang, *Adv. Mater.* **2020**, *32*, 1906712; g) T. Ma, T. Li, L. Zhou, X. Ma, J. Yin, X. Jiang, *Nat. Commun.* **2020**, *11*, 1811; h) Z. Li, X. Liu, G. Wang, B. Li, H. Chen, H. Li, Y. Zhao, *Nat. Commun.* **2021**, *12*, 1363; i) Y. Liu, S. Liang, C. Yuan, A. Best, M. Kappl, K. Koynov, H. J. Butt, S. Wu, *Adv. Funct. Mater.* **2021**, *31*, 2103908; j) C. N. Zhu, C. Y. Li, H. Wang, W. Hong, F. Huang, Q. Zheng, Z. L. Wu, *Adv. Mater.* **2021**, *33*, 2008057.

[8] a) X. Hou, C. Ke, C. J. Bruns, P. R. McGonigal, R. B. Pettman, J. F. Stoddart, *Nat. Commun.* **2015**, *6*, 6884; b) H. Wang, X. Ji, Z. Li, C. N. Zhu, X. Yang, T. Li, Z. L. Wu, F. Huang, *Mater. Chem. Front.* **2017**, *1*, 167; c) X. Ji, R. T. Wu, L. Long, X. S. Ke, C. Guo, Y. J. Ghang, V. M. Lynch, F. Huang, J. L. Sessler, *Adv. Mater.* **2018**, *30*, 1705480; d) Y. Zhang, X. Le, Y. Jian, W. Lu, J. Zhang, T. Chen, *Adv. Funct. Mater.* **2019**, *29*, 1905514; e) Y. Ma, F. Yu, S. Zhang, P. She, S. Liu, W. Huang, Q. Zhao, *CCS Chem.* **2020**, *2*, 2437; f) Y. Sagara, H. Traeger, J. Li, Y. Okado, S. Schrettl, N. Tamaoki, C. Weder, *J. Am. Chem. Soc.* **2021**, *143*, 5519; g) X. Yao, J. Wang, D. Jiao, Z. Huang, O. Mhirsi, F. Lossada, L. Chen, B. Haehnle, A. J. C. Kuehne, X. Ma, H. Tian, A. Walther, *Adv. Mater.* **2021**, *33*, 2005973.

[9] a) S. Zeng, D. Zhang, W. Huang, Z. Wang, S. G. Freire, X. Yu, A. T. Smith, E. Y. Huang, H. Nguon, L. Sun, *Nat. Commun.* **2016**, *7*, 11802; b) Z. Gao, Y. Han, F. Wang, *Nat. Commun.* **2018**, *9*, 3977; c) W. Tian, J. Zhang, J. Yu, J. Wu, J. Zhang, J. He, F. Wang, *Adv. Funct. Mater.* **2018**, *28*, 1703548; d) D. Tian, Z. Zhu, L. Xu, H. Cong, J. Zhu, *Mater. Horiz.* **2019**, *6*, 1215; e) S. Liu, Y. Cheng, Y. Li, M. Chen, J. W. Y. Lam, B. Z. Tang, *ACS Nano* **2020**, *14*, 2090; f) D. Lu, M. Zhu, S. Wu, Q. Lian, W. Wang, D. Adlam, J. A. Hoyland, B. R. Saunders, *Adv. Funct. Mater.* **2020**, *30*, 1909359; g) Y. Yao, C. Yin, S. Hong, H. Chen, Q. Shi, J. Wang, X. Lu, N. Zhou, *Chem. Mater.* **2020**,

32, 8868; h) R. Lan, Y. Gao, C. Shen, R. Huang, J. Bao, Z. Zhang, Q. Wang, L. Zhang, H. Yang, *Adv. Funct. Mater.* **2021**, *31*, 2010578; i) Y. Liu, Y. Zhang, *ACS Nano* **2021**, *15*, 7628; j) W. Lu, M. Si, H. Liu, H. Qiu, S. Wei, B. Wu, R. Wang, G. Yin, J. Zhang, P. Theato, Y. Wei, T. Chen, *Cell Rep. Phys. Sci.* **2021**, *2*, 100417.

[10] a) R. A. Potyrailo, H. Ghiradella, A. Vertiatchikh, K. Dovidenko, J. R. Cournoyer, E. Olson, *Nat. Photonics* **2007**, *1*, 123; b) E. A. Widder, *Science* **2010**, *328*, 704; c) Y. Wang, H. Cui, Q. Zhao, X. Du, *Matter* **2019**, *1*, 626.

[11] L. M. Mathger, E. J. Denton, N. J. Marshall, R. T. Hanlon, *J. R. Soc. Interface* **2009**, *6*, S149.

[12] a) X. He, M. Aizenberg, O. Kuksenok, L. D. Zarzar, A. Shastri, A. C. Balazs, J. Aizenberg, *Nature* **2012**, *487*, 214; b) A. Shastri, L. M. McGregor, Y. Liu, V. Harris, H. Nan, M. Mujica, Y. Vasquez, A. Bhattacharya, Y. Ma, M. Aizenberg, O. Kuksenok, A. C. Balazs, J. Aizenberg, X. He, *Nat. Chem.* **2015**, *7*, 447.

[13] a) L. Hu, Y. Wan, Q. Zhang, M. J. Serpe, *Adv. Funct. Mater.* **2019**, *30*, 1903471; b) L. Hu, Q. Zhang, X. Li, M. J. Serpe, *Mater. Horiz.* **2019**, *6*, 1774.

[14] J. Yu, K. Wang, C. Fan, X. Zhao, J. Gao, W. Jing, X. Zhang, J. Li, Y. Li, J. Yang, W. Liu, *Adv. Mater.* **2021**, *33*, 2008395.

[15] M. Si, H. Shi, H. Liu, H. Shang, G. Yin, S. Wei, S. Wu, W. Lu, T. Chen, *Mater. Chem. Front.* **2021**, *5*, 5130.

[16] K. Binnemans, *Chem. Rev.* **2009**, *109*, 4283.

[17] S. Wei, H. Qiu, H. Shi, W. Lu, H. Liu, H. Yan, D. Zhang, J. Zhang, P. Theato, Y. Wei, T. Chen, *ACS Nano* **2021**, *15*, 10415.